mRNA localisation in endothelial cells regulates blood vessel sprouting

Guilherme Costa[1], Nawseen Tarannum[1] and Shane P. Herbert[1*]

[1]Faculty of Biology, Medicine and Health, The University of Manchester, Manchester, M13 9PT, UK

*Correspondence:

shane.herbert@manchester.ac.uk (S.P.H.)

SUMMARY

The subcellular distribution of mRNAs is a fundamental biological mechanism implicated in the spatial regulation of gene expression in many cellular contexts. However, whether mRNA localisation contributes to complex morphogenetic processes underpinning tissue development remains unknown. We focused on a model transcript, *RAB13*, and demonstrated how it is preferentially localised to and locally translated at the leading edge of migrating endothelial cells. We generated a novel MS2-GFPnls zebrafish reporter strain and use the 3' UTR of *RAB13* to show, for the first time, tissue-specific visualisation of a localised RNA in migratory cell processes in a living vertebrate organism. Moreover, after mutating the endogenous 3' UTR of *RAB13* to disrupt transcript localisation *in-vivo,* we report altered formation of endothelial cell protrusions within sprouting vessels. Hence, we demonstrate the involvement of mRNA localisation in endothelial cell migration during angiogenesis and are the first to reveal that subcellular transcript distribution modulates tissue morphogenesis.

INTRODUCTION

mRNA localisation is a well-established and crucial determinant of cell polarity (Buxbaum et al., 2015). Subcellular distribution of transcripts restricts translation to particular locations within the cell and it has been suggested to facilitate local protein activity. This mode of spatial control of gene expression contributes to rapid and localised cellular responses with implications in development and disease (Chin and Lecuyer, 2017). Although many of the protein-mediated mechanisms that regulate cell migration are well understood, only a handful of studies have delved thoroughly into the implications of mRNA localisation in cell movement (Kislauskis et al., 1994, 1997; Liao et al., 2011; Schedlich et al., 1997; Shestakova et al., 2001; Wang et al., 2017). Much effort has been dedicated to understanding *β-ACTIN* mRNA localisation, a transcript typically enriched at the leading front of motile cells and whose subcellular distribution is mediated by a short element in its 3' UTR (Kislauskis et al., 1994, 1997; Liao et al., 2011; Park et al., 2014; Schedlich et al., 1997; Shestakova et al., 2001; Wang et al., 2017). Nevertheless, these findings have been limited to *in vitro or ex vivo* observations, as live visualisation of mRNA distribution in complex organisms is challenging. Moreover, despite the recent application of methods developed to image RNA localisation in yeast cells (Bertrand et al., 1998) being applied to visualise RNAs in zebrafish embryonic cells (Campbell et al., 2015), the dynamic subcellular spatial localisation of mRNAs *in-vivo* and function in coordinating complex morphogenetic events, such as angiogenesis, remains unexplored.

Most new blood vessels emerge through angiogenic sprouting, an intricate morphogenetic process that entails the coordinated migration of endothelial cells branching from parental vessels

(Herbert and Stainier, 2011). Critical guidance cues such as the Vascular Endothelial Growth Factor (VEGF) secreted by the surrounding tissues regulate the molecular and cellular responses of endothelial cells triggered during angiogenesis (Gerhardt et al., 2003; Ruhrberg et al., 2002). Similar to other collective cell migration systems (Mayor and Etienne-Manneville, 2016), endothelial cells within sprouting vessels are hierarchically organised into leader tip cells and follower stalk cells (Arima et al., 2011; Gerhardt et al., 2003). Tip cells are highly polarised, presenting a leading edge that extends filopodia-containing protrusions and interacts with the extracellular matrix, whilst their rear engages in cell-to-cell contacts with stalk cells (Bentley et al., 2014; Gerhardt et al., 2003). Asymmetric distribution of cytoplasmic components contributes to dynamic membrane remodelling phenomena that are constrained to the cell-leading front during migration (Krause and Gautreau, 2014). Moreover, this inherent asymmetry is crucial for the maintenance of cell hierarchies following tip cell division during blood vessel growth (Costa et al., 2016). Whether the subcellular distribution of mRNAs is part of the polarity-defining asymmetry that controls endothelial cell migration during angiogenesis is unknown.

RAB13 belongs to the large RAB family of proteins, small GTPases that act as molecular switches controlling intracellular vesicle trafficking in many biological processes (Bhuin and Roy, 2014). Firstly reported as a key modulator of tight junction maintenance in epithelial cells (Marzesco et al., 2002; Zahraoui et al., 1994), RAB13 participates in cytoskeletal remodelling through the activity of its effector protein MICAL-L2 (Sakane et al., 2012; Sakane et al., 2013). RAB13 changes the conformational structure of MICAL-L2, which in turn interacts with the actin-binding proteins of the Filamin family and ultimately leading to membrane rearrangements at the leading edge of migrating cells (Sakane et al., 2013). More recently, Ioannou et al. (2015) have elegantly shown with biosensor tools that the RAB13 guanine exchange factor (GEF) DENND2B switches RAB13 into its active form at the leading edge of invasive tumour cells. The role of RAB13 in migration has also been demonstrated in VEGF-guided motility of endothelial cells. In this context, RAB13-mediated trafficking delivers the GEF Syx to the cell front, where together with its substrate RhoA modulates endothelial cell migration (Wu et al., 2011). Although RAB13 mRNA has been previously identified in protrusions formed at the front of migrating fibroblasts and tumour cells (Jakobsen et al., 2013; Mardakheh et al., 2015; Mili et al., 2008), the *in-vivo* morphogenetic function of the intracellular targeting of *RAB13* mRNA (or indeed any other mRNA) is currently unknown.

Here, we sought to investigate whether subcellular targeting of mRNAs defines a novel paradigm for the dynamic control of tissue morphogenesis. Using angiogenesis as a model morphogenetic system, we performed a transcriptome-wide screen of mRNAs enriched in protrusions formed at the leading edge of endothelial cells and identified *RAB13* as one of the most abundant transcripts. Visualisation of *RAB13* mRNA unveiled an extraordinary polarisation towards the migratory front of

angiogenic endothelial cells, as well as local translation. Moreover, using novel vascular-specific reporter transgenics and live imaging in zebrafish, we show for the first time the dynamic localisation of targeted mRNAs to migratory protrusions *in vivo*. Finally, to assess the functional role of localised *rab13* transcripts in this context, we generated a zipcode-deleted mutant zebrafish strain and report abnormal protrusion formation and migratory dynamics of sprouting embryonic vessels. Hence, we reveal for the first time that polarised targeting of mRNAs, and not just their expression, modulates directional motile cell behaviour to dictate tissue morphogenesis in a vertebrate organism.

RESULTS

The endothelial cell transcriptome is asymmetrically distributed during migration.

Extensive research over the last two decades has established the subcellular localisation of mRNA as a key determinant in the spatial regulation of gene expression (Chin and Lecuyer, 2017). To start investigating the implications of this biological mechanism in endothelial cell migration and angiogenesis, we carried out a series of assays culturing Human Umbilical Vein Endothelial Cells (HUVECs) in modified Boyden chambers (Boyden, 1962) (hereafter referred as Transwells). This experimental setup allows the leading edge of migrating cells to extend protrusions through porous membranes separating two media-containing chambers and has been widely used to isolate compartmentalised mRNAs from diverse cell types (Jakobsen et al., 2013; Mili et al., 2008; Stuart et al., 2008; Zappulo et al., 2017). HUVECs were cultured for 2 hours in the upper chambers of Transwells containing 3µm pore membranes, in low serum conditions. Subsequently, VEGF-A was added to the lower Transwell chamber to promote cell migration through the membranes (Lee et al., 2002) during the following hour (**Figure 1A**). The short culture periods permits the formation of protrusions during the initial stages of migration into the lower chambers whilst the cell bodies remain in the upper chamber. In order to investigate whether HUVECs preferentially localise transcripts to their leading edge, RNA was extracted from cell bodies and protrusions to perform a high-throughput screen (RNA-seq). In these studies, we identified a set of 320 mRNAs enriched in HUVEC protrusions (fold change >1.6) when compared to mRNAs present in the cell body fraction (**Figure 1B**). Many of the mRNAs we detected in protrusions encode proteins that regulate cell motility and have also been identified as transcripts preferentially localised to the leading edge of highly migratory cells. One of these transcripts encodes *RAB13*, a small GTPase associated with cell membrane dynamics underlying cell migration (Ioannou et al., 2015; Sakane et al., 2013), which was amongst the transcripts with the highest levels of enrichment in HUVECs (**Figures 1B** and **1C)**. On the other hand, while the classical protrusion-related *β-ACTIN* mRNA presented a rather modest enrichment,

transcripts encoding the membrane-bound VEGFR2 were more abundant in cell bodies (**Figures 1B** and **1C**). Interestingly, we noted that no other transcripts encoding RAB proteins expressed in HUVECs were enriched in protrusions (**Figure 1B**). These distinctive aspects of *RAB13* prompted us to study it as a model for localised mRNA function in migrating endothelial cells.

***RAB13* mRNA is localised at the distal end of tip cells during angiogenesis.**

To characterize in detail the subcellular distribution of *RAB13* transcripts, we performed single molecule fluorescent *in situ* hybridisation (smFISH) using HUVECs maintained in different culture contexts. Firstly, sparse cells cultured in 2D surfaces were fixed and hybridised with probes recognising *RAB13* mRNA in combination with probes detecting the control transcript *GAPDH* (**Figure 1D, Figure S1A**). The transcript distribution was subsequently quantified using an analytical method developed by Park et al. (2012) for cell cultures in 2D, which measures the displacement of the centre of mRNA distribution from the cell centre in the form of a Polarisation Index (PI). These experiments showed a striking asymmetric distribution of *RAB13* mRNA (PI 0.67) when compared *GAPDH* mRNA (PI 0.24) in a randomly sampled population of individual HUVECs (**Figure 1E**). Next, to study transcript localisation in the context of collective endothelial cell migration, we carried out smFISH using scratch wound assays to compare mRNA distribution in leader cells with follower cells. To do so, HUVECs were cultured to confluence and a wound was induced to promote oriented migration towards the cleared space. Leader cells present at the wound edge showed an increased *RAB13* mRNA polarisation level (PI 0.76) than cells follower cells located in confluent areas (PI 0.50) (**Figures S1C-S1G)**. Interestingly, the mean number of smFISH spots detected in leader cells (70 spots) was significantly higher than in follower cells (42 spots) indicating that leader cells upregulate *RAB13* (**Figure S1H)**.

Although the scratch wound assay generates leader and follower cells and confers directionality to collectively migrating cells, it does not recapitulate many of the complex mechanism that take place in 3D physiological environments during angiogenesis. Hence, to visualise and characterise the subcellular distribution of *RAB13* mRNA in cells at the leading front of growing blood vessels, we opted to perform *in vitro* angiogenesis assays. Microbeads coated with HUVECs were cultured in a fibrin matrix covered by a monolayer of fibroblasts to promote the chemotactic angiogenic sprouting (Nakatsu and Hughes, 2008). Remarkably, the distal-most region of tip leader cells within sprouts showed a strong accumulation of *RAB13* mRNA (**Figure 1F, Figure S1B**). Given that assessing transcript PIs in 3D proved technically challenging, we measured the relative distance between the centre of mRNA distribution and the cell nucleus to compare the distribution of *RAB13* and *GAPDH* transcripts. Applying this method, we observed that *RAB13* mRNA displayed a higher distal distribution (relative distance 0.54) than *GAPDH* mRNA (relative distance 0.33) (**Figure 1G**).

Altogether, these observations not only validate the RNA-seq data but also led us to further investigate the implications of *RAB13* mRNA localisation in angiogenesis.

RAB13 is translated at the leading edge of endothelial cells during migration

To verify whether translation of local mRNAs can take place in protrusions formed at the leading edge of endothelial cells, HUVECs were cultured in Transwells as described above and Puromycin was briefly added the to lower chambers at the end of the assay. Puromycin incorporates nascent peptide chains and labels newly translated proteins that can be recognised by immuno-detection. HUVEC protrusions containing puromycinilated proteins were found in the lower side of Transwells membranes but not in those cultured without Puromycin or those co-treated with the translation inhibitor Anisomycin (**Figure S2A**). To exclude potential puromycinilation of proteins synthesised by cell bodies and transported into protrusions, the former were removed prior to a short incubation with or without Puromycin or with a combination of Puromycin and Anisomycin (**Figure 2A**). Likewise, protrusions containing puromycinilated proteins were detected in cell body-free Transwell membranes exposed to Puromycin, but not when also treated with Anisomycin (**Figure 2B**). Our observations indicated HUVEC protrusions contain active translational machinery that synthesises proteins independently of cell bodies. However the puromycylation of newly synthesised proteins can be further used in combination with antibody-based proximity ligation assays (Puro-PLA) to detect local translation of proteins of interest (tom Dieck et al., 2015). To test whether RAB13 is locally translated, Puro-PLA experiments were performed with HUVEC protrusions segregated from cell bodies. Using antibodies targeting RAB13 and Puromycin, we observed higher levels of PLA signal (0.01 punctae/μm^2) in protrusions exposed to Puromycin than those in Puromycin-free control cultures (0.002 punctae/μm^2) (**Figures 2C** and **2D**) or in the absence of antibodies (0.001 punctae/μm^2) (**Figure S2B and S2C)**. Upon treatment with Anisomycin, the PLA signal was significantly reduced (0.004 punctae/μm^2) (**Figures 2C** and **2D**). In summary, these results demonstrate that *RAB13* and likely other mRNAs are spatially targeted to and actively translated at the leading of migratory endothelial cells.

Identification of a *RAB13* mRNA zipcode sequence that localises transcripts *in vitro* and *in vivo*.

Localisation elements mediating the subcellular distribution of mRNAs are commonly found within 3' UTRs (Andreassi et al., 2010; Aschrafi et al., 2010; Brittis et al., 2002; Kislauskis et al., 1994; Mili et al., 2008; Wu et al., 2005). In fact, the 3' UTR of the mouse *RAB13* orthologue has been shown to localise transcripts to protrusion of mouse fibroblasts (Mili et al., 2008) using the MS2 system developed by the Singer lab (Bertrand et al., 1998), but the specific "zipcode" sequence responsible is unknown. With the MS2 modular tool, RNA regions of interest are tagged with repeats of the

bacteriophage-derived MS2 hairpin, a high affinity sequence for the MS2 capping protein (MCP). Subsequently, MCP fused to the green fluorescent protein (MCP-GFP) is co-expressed in the cell of interest with MS2 tagged RNA to investigate transcript behaviour in living cells. To begin to define the *RAB13* 3' UTR localisation element, we cloned the 3' UTR downstream of a cassette containing 24 MS2 hairpins and co-transfected it with a nuclear from of MCP-GFP(nls) into endothelial cells. Whilst in control transfections MCP-GFPnls expression was restricted to the nucleus, cells transfected with MS2-tagged *RAB13* 3' UTR formed protrusions with local accumulation of MCP-GFPnls (**Figure 3A**). Moreover, deleting fragments within the *RAB13* 3' UTR revealed that minimal region between nucleotide positions 90-282(nt) within *RAB13* 3' UTR was sufficient to localise MCP-GFPnls to endothelial cell protrusions (**Figures 3B** and **S3A**). Next, to examine whether this region is indeed responsible for the subcellular distribution of endogenous transcripts, we used CRISPr/Cas9 tools to excise it from the genomic *RAB13* locus of HUVECs (**Figure S3B)**. In contrast to control cells that maintained the characteristic localisation of *RAB13* mRNA, CRISPr-edited HUVECs showed a remarkable reduction in the accumulation of *RAB13* transcripts in protrusions (**Figures 3C** and **S3C**) and decreased *mRNA* polarisation levels (**Figures 3D**).

The zebrafish embryo is a powerful and well-established tool to study angiogenesis and many fluorescent transgenic strains have been generated to visualise the development of blood vessels in living animals (Hogan and Schulte-Merker, 2017). Hence, we set out to study whether the zebrafish *RAB13* 3' UTR othologue also localises transcripts in endothelial cells during embryonic vascular development to further understand the *in-vivo* implications of asymmetric mRNA distributions in tissue morphogenesis. To visualise the localisation of *rab13* mRNA *in vivo* during angiogenesis, we generated a vascular-specific MCP-GFPnls transgenic zebrafish strain [*Tg(fli1ep:MCP-GFPnls*)] (**Figure S3D**). Single cell stage transgenic embryos were injected with a construct containing the zebrafish *rab13* 3' UTR downstream of 24 MS2 hairpins and the membrane-targeted fluorescent protein Lyn-mCherry (**Figure S3E**). One day later, embryos with mosaic expression of Lyn-mCherry were examined using confocal imaging. We focused on intersegmental vessels (ISVs), a well-characterised vessel bed that sprouts from the embryonic dorsal aorta (Isogai et al., 2003). In these embryos, Lyn-mCherry-expressing endothelial cells within ISVs displayed a striking accumulation of MCP-GFPnls in distal protrusions that extended towards the dorsal side of the embryo (**Figure 3E**). The distribution of MCP-GFPnls in endothelial cell protrusions was extremely dynamic, reflecting the rapid remodelling of the cell membrane during migration. This non-nuclear localisation of MCP-GFPnls demonstrates that the elements present in the *rab13* 3' UTR localise transcripts to the leading edge of angiogenic endothelial cells *in vivo.* Importantly, our pioneering data show, for the first time, tissue-specific visualisation of mRNA localisation within a living vertebrate organism.

The asymmetrical distribution of *rab13* mRNA fine-tunes angiogenic sprouting

Following our *in vivo* observations, we sought to investigate the role of *rab13* mRNA localisation during endothelial cell migration in zebrafish embryos. The use of genetic tools to delete 3' UTRs has been a strategy successfully used in studying the implications of subcellular transcript localisation in neurons (An et al., 2008; Miller et al., 2002). However, *in vivo* functional roles for localised mRNAs in tissue migration and vertebrate morphogenesis have not been explored. Thus, we applied CRISPr/Cas9 technology to delete a 482nt fragment of the *rab13* 3' UTR that we predicted may encode the mRNA targeting sequence (**Figure S4A**). This deletion was generated in the zebrafish *Tg(flk1:EGFP)*^{s843} transgenic background to facilitate the visualisation of developing blood vessels (Jin et al., 2005). Breeding heterozygous animals generated progeny with expected Mendelian frequencies (**Figures S4B** and **S4C)** and with no significant changes in the relative levels of *rab13* mRNA at 22-26 hours post fertilisation (hpf) (**Figure S4D)**. In order to confirm that disrupting the 3' UTR of *rab13* results in transcript mislocalisation, 24 hpf embryos obtained from incrossed heterozygous *rab13* 3' UTR-deleted zebrafish were dissociated and cultured for 18 hours and analysed with smFISH assays. The polarisation levels of *rab13* mRNA were significantly reduced in homozygous cells (PI 0.35) when compared to wild type counterparts derived from sibling embryos (PI 0.53) (**Figures 4A** and **4B),** whilst heterozygous cells displayed intermediate levels (PI 0.43) (**Figure 4B)**. Having demonstrated that the 3' UTR of zebrafish *rab13* mediates endogenous transcript distribution, we next assessed whether mislocalising *rab13* affects angiogenic sprouting in zebrafish embryos. Thus, time-lapse confocal microscopy was used to image developing ISVs in sibling embryos generated from *rab13* 3' UTR heterozygous *Tg(flk1:EGFP)*^{s843} fish. While no substantial differences in ISV length were detected in any genotypes (**Figure S4E)**, homozygous *rab13* 3' UTR embryos showed a higher frequency (66%) of ISVs containing transient vessel branches emerging from the main ISV sprout than heterozygous (45%) and wild type (33%) counterparts (**Figures 4C** and **S4F)**. Furthermore, we observed that ectopic branching typically occured at the leading front of sprouting vessels in two main embryonic regions: 1) close to the dorsal side of the embryo, immediately before the ISVs form of the dorsal longitudinal anastomotic vessel (DLAV) and 2) close to the horizontal myoseptum (HM) at the earlier stages of the ISV spouting process (**Figure 4D)**. These types of branching may reflect different stages of decision-making processes that endothelial cells face during guided migration to correctly form blood vessels. Indeed, transient vessel branching at the dorsal side of the embryo close to the DLAV was a common feature of WT branching, suggesting a lack of clear directionality in the later stages of ISV sprouting. However, ISVs presenting transient branches close to HM were uncommon in wild types and were detected with much higher frequencies in homozygous *rab13* 3' UTR embryos (64%) than in heterozygous (19%) and wild type siblings (13%) (**Figure 4E)**. Hence, normal guidance of

developing vessels is dependent upon the intracellular targeting of *rab13* mRNA and not expression of the transcript *per se*. Altogether, these results demonstrate that the 3' UTR of *rab13* is crucial for its localisation *in vivo* and the control of endothelial cell guidance. Moreover, we reveal for the first time that the correct subcellular distribution of mRNAs is a novel paradigm for the coordination of vertebrate tissue morphogenesis.

DISCUSSION

The polarisation of cellular components is a key cellular feature during migration. Polarised cells actively remodel their microfilament network at their leading edge resulting in an array of rapid and dynamic rearrangements of the plasma membrane. Thus, the formation of membrane protrusions at the leading edge mediates migration guidance in response to microenvironmental cues (Krause and Gautreau, 2014). During angiogenesis, polarised endothelial cells migrate collectively to form new blood vessels. In addition, we have recently shown that highly polarised tip cells at the leading front of sprouting vessels divide asymmetrically to maintain their critical polarised properties during coordinated migration (Costa et al., 2016). Here, we unveil that mRNAs are asymmetrically distributed in migratory endothelial cells and that the subcellular localisation of *RAB13* transcripts is implicated in protrusion formation during blood vessels growth.

In groups of endothelial cells undergoing collective cell migration, leader cells not only show higher polarisation of *RAB13* mRNA but also contain increased *RAB13* transcript levels. Although motile HUVECs express many of the genes encoding RAB proteins, only *RAB13* transcripts are highly enriched in protrusions. This not only suggests a transcript-specific role for the asymmetric *RAB13* mRNA distribution but also offers an excellent model transcript to study mRNA localisation in angiogenesis. Similarly to endothelial cells, the presence of *RAB13* mRNA at the leading edge has been previously reported in diverse cell types (Jakobsen et al., 2013; Mili et al., 2008; Zappulo et al., 2017), suggesting that the localisation of these transcripts may be part of the conserved machinery regulating cell migration. Nevertheless, a detailed understanding of the mechanisms of mRNA localisation and their implications in complex morphogenetic processes had yet to be addressed. The localisation of *RAB13* mRNA is an evolutionary conserved process that occurs via localisation elements present in the 3' UTR. Whilst the targeting properties of *RAB13* 3' UTR have been firstly identified in its murine orthologue (Mili et al., 2008), here we have defined the specific targetting region responsible and demonstrated that the equivalent regions of the zebrafish mRNA drive localisation of transcripts to protrusions formed at the leading edge of migrating cells *in vivo*. Furthermore, the deletion of this region *in vivo* induces the formation of extra branching at the leading

front of zebrafish ISVs at early stages of embryonic vessel sprouting, revealing that the 3' UTR-mediated localisation of *RAB13* mRNA (but not its expression *per se*) is involved in cell path finding. It is tempting to speculate that the accumulation of *RAB13* mRNA in the correct subcellular domain allows the persistence of protrusions along the correct migration path, in detriment of alternative protrusion formation at the leading front of the vessel. The transport of *RAB13* transcripts in fibroblast protrusions has been partly attributed to the adenomatous polyposis coli (APC) (Mili et al., 2008; Wang et al., 2017), a tumour suppressor protein found at the leading front of endothelial cells (Harris and Nelson, 2010). Whether APC interacts directly with the 3' UTR or indirectly through other RNA binding proteins and how this is regulated in endothelial cell migration is yet to be addressed.

The proportion of protrusion-enriched mRNAs that undergo translation has been reported with disparity in distinct cell types. While Mardakheh et al. (2015) suggested that most mRNAs enriched in tumour cell protrusions are in fact translationally repressed, Zappulo et al. (2017) reported that a great part of the transcripts localised to neuronal processes undergo translated. Using an *in situ* visualisation approach, we verified that *RAB13* mRNA is actively translated in endothelial protrusions independently of the cell body, indicating that the localisation of the transcript provides a pool of newly synthesised RAB13 to the leading edge the cell. The synthesis of RAB proteins in the cytosol has been proposed to contribute to a pool of newly translated RAB proteins different from pre-existing ones that display distinct interacting partners (Seabra et al., 2002). RAB escorting proteins (REPs) interact with newly synthesised RAB proteins in the cytosol to promote its prenylation and consequently, association with vesicular membranes (Shen and Seabra, 1996). On the other hand, pre-existing RAB proteins bound to GDP are displaced from membranes by the GDP dissociation inhibitor (GDIs) and targeted for recycling (Pfeffer et al., 1995). The ability of REPs and GDIs to differentially regulate the two pools may result in distinct biological outcomes. It is plausible that newly translated *RAB13* in its unmodified form is rapidly available to be deposited in membrane vesicles and exert its molecular control of microfilament rearrangement at leading edge of migrating cells. Alternatively, localised translation could simply increase the local concentration of RAB13 presented to its activator GEFs in protrusions. Hence, in our angiogenesis studies, the absence of polarised *rab13* transcripts in zebrafish embryos would reduce local amounts of newly synthesised protein, resulting in abnormal protrusion formation during blood vessel sprouting.

In summary, the studies presented here provide novel insights into the involvement of subcellular mRNA localisation in complex morphogenetic events *in vivo* and define a new paradigm for the cellular control of directional blood vessel growth and vertebrate tissue morphogenesis.

AUTHOR CONTRIBUTIONS

Conceptualisation, G.C. and S.P.H.; Methodology, G.C.; Formal Analysis, G.C.; Investigation, G.C. and N.T.; Writing – original draft, G.C.; Writing – review and editing, S.P.H.; Supervision, G.C. and S.P.H.; Funding acquisition, S.P.H.

ACKNOWLEDGMENTS

We wish to thank members of the Biological Services, Genomic Technologies and Bioimaging Facilities at the FBMH, University of Manchester, for technical support. We also thank N. Papalopulu and members of for her research group at the FBMH, University of Manchester, for critical feedback and for providing reagents and materials. This work was funded by the Wellcome Trust (095718/Z/11/Z to S.P.H.), Wellcome Institutional Strategic Support Fund (7064646 to G.C.) and the British Heart Foundation (PG/16/2/31863 to S.P.H.).

DECLARATION OF INTERESTS

The authors declare no competing interests

METHODS

Zebrafish husbandry

Zebrafish were maintained and bred according to standard conditions. Experimental procedures were approved by the University of Manchester Ethical Review Board and performed according to UK Home Office regulations.

Embryo micro-injections and generation of zebrafish strains

To generate the transgenic zebrafish strain *Tg(fli1ep:MCP-GFPnls*), 32 pg of Cerulean-H2B:bas*fli1ep*:MCP-GFPnls Tol2-based plasmid was co-injected with 32 pg Tol2 mRNA into one cell stage AB zebrafish embryos. The next day, embryos with mosaic GFP expression were selected, raised into adulthood and then outbred to AB zebrafish to identify founders with germ-line transmission of the transgene. Adult *Tg(fli1ep:MCP-GFPnls*) were inbred and one cell stage embryos were co-injected with 32 pg of Cerulean-H2B:bas*fli1ep:*Lyn-mCherry-24xMS2-rab13-3'UTR Tol2-based plasmid and 32 pg Tol2.

The mutant Δ482 *rab13* 3' UTR strain was generated with CRISPr/Cas9 tools. One cell stage *Tg(flk1:EGFP)*^{s843} embryos were injected with 150 pg of each *in vitro* transcribed gRNAs and co-injected with 150 pg Cas9 NLS nuclease (New England Biolabs). Embryos were raised into adulthood and outbred to AB zebrafish to identify founders with germ-line transmission of a mutant *rab13* 3' UTR.

gRNA generation and *in vitro* translation

The online CRISPRscan tool was used to design gRNAs targeting the zebrafish 3' UTR region in the *rab13* locus (Moreno-Mateos et al., 2015). Oligonucleotides comprising the target sequences flanked by the T7 promoter and the Tail annealing sequence (Moreno-Mateos et al., 2015) were annealed to the Tail primer in a T100 thermal cycler (BioRad).

The SP6 and T7 mMESSAGE mMACHINE kits (Thermo Fisher) were used according to transcribe 1 µg NotI-linearised pCS-TP plasmid and annealed 400 ng gRNA oligonucleotides, respectively.

Embryo genotyping

Genomic DNA was extracted incubating embryos in lysis buffer (10mM Tris HCl pH8, 1mM EDTA, 80mM KCl, 0.3% NP40, 0.3% Tween) containing 0.5 µg/µl Proteinase K (Promega) at 55°C for 1-2 hours followed and 95°C for 15 minutes in a T100 thermal cycler. Genotyping PCR was performed using 2 µl genomic DNA, 0.4 µM zebrafish genotyping primers (Figure S4A) and 1 x MyTaq Red

DNA Polymerase (Bioline) according to the manufacturer's protocol in a T100 thermal cycler. PCR reactions were loaded in 1 % agarose gels containing 0.5 µg/ml Ethidium Bromide (Sigma).

Embryo cell culture

Trunks of 26-28 hpf embryos were incubated in Trypsin-EDTA solution (Sigma) at 28°C for 15 minutes. Trypsinisation was quenched with L-15 medium (Sigma) containing 10 % Fetal Bovine Serum (FBS, Sigma). Cells were pelleted at 2000 rpm for 5 minutes, resuspended in L-15 medium containing 10 % Fetal Bovine Serum, plated on Laminin (Sigma) coated coverslips and maintained at 28°C.

Cell culture, cell transfections and CRISPr/Cas9 cell editing

HUVECs (PromoCell) were cultured in complete ECGM2 (PromoCell) in gelatin (Millipore) coated dishes. Human Pulmonary Fibroblasts (HPF, PromoCell) were cultured in M199 (Thermo Fisher) containing 10 % FBS, 50 µg/ml gentamycin (Sigma) and 50 ng/ml amphotericin (Sigma). Brain endothelial (bEnd.3) were cultured in DMEM (Sigma) supplemented with 10 % FBS, 10 ng/ml Recombinant Human VEGF-A (PeproTech) and 10 U/ml-100µg/ml Penicillin-Streptomycin (Sigma). Both cell types were maintained in standard culture conditions, with 5% CO_2 at 37°C.

To edit the 90-182nt within the 3' UTR region of the *rab13* locus, HUVECs were transfected with Alt-R CRISPr/Cas9 ribonucleotide complexes (Integrated DNA Technologies) following the manufacturer's manual, using a Nucleofector 2b Device (Lonza). Transfections were performed in cuvettes of a HUVEC Nucleofector kit (Lonza) and 2 µg pmaxGFP was added to the HUVEC-ribonucleotide mix to identify transfected cells. Single GFP expressing cells were isolated in a FACS Aria Fusion cell sorter (BD Biosciences) into gelatin-coated 96 well plates. Genomic DNA was extracted from expanded HUVEC clones and analysed as described for embryo genotyping using human genotyping primers.

For MS2 experiments *in vitro,* bEnd.3 were cultured in 6 well plates at $100x10^3$ cells / well and transfected with a total of 2.4µg plasmid DNA using Lipofectamin2000 following the manufacturer's protocol (Thermo Fisher). The following plasmids were co-transfected: pcDNA3-Lyn-mCherry, pMS2-GFP, a gift from Robert Singer (Addgene plasmid # 27121) (Fusco et al., 2003) and different versions of pcDNA3-24XMS2SL-*RAB13* 3' UTR.

Transwell assays, cell body / protrusion fractionation

Transwell experiments to segregate cell bodies and protrusions were performed as described elsewhere (Mili et al., 2008), with the following modifications: HUVECs were cultured for 2 hours in Transwells (Costar) containing M199 (Thermo Fisher) supplemented with 1 % FBS in both upper

and lower chambers. Subsequently, 25ng/ml VEGF-A was added to the lower chambers to promote cell migration over the next hour.

RNA isolation, qPCR and RNA-seq

Embryo and cell-derived RNA was isolated using a RNAqueous-Micro Kit (Thermo Fisher) according to the manufacturer's protocol. For gene expression analysis, cDNA was synthesised with a High –Capacity RNA-to-cDNA kit (Thermo Fisher) following the manufacturer's protocol

qPCR experiments were performed with 1-2 µl cDNA, 0.25 µM gene-specific primers and 1 x Power SYBR Green Master Mix (Thermo Fisher) in a StepOne Real-Time PCR System (Applied Biosystems). Either human or zebrafish *GAPDH* expression was used to normalise gene expression levels.

For RNA-seq, quality and integrity of RNA samples obtained from HUVEC cell bodies and protrusions were assessed using a 2200 TapeStation (Agilent Technologies). Next, RNA-seq libraries were generated using the TruSeq Stranded mRNA assay (Illumina) according to the manufacturer's protocol. Adapter indices were used to multiplex libraries, which were pooled prior to cluster generation using a cBot instrument. The loaded flow-cell was then paired-end sequenced (76 + 76 cycles, plus indices) on an Illumina HiSeq4000 instrument. Finally, the output data was demultiplexed (allowing one mismatch) and BCL-to-Fastq conversion performed using Illumina's bcl2fastq software, version 2.17.1.14

Fibrin sprout assay and scratch wound assay

Fibrin sprout assays were performed as previously described by Nakatsu and Hughes (2008). HUVECs cultured on gelatin coated coverslips were grown to confluence and used in scratch wound assays as described elsewhere (Liang et al., 2007).

smFISH

Zebrafish cells, HUVECs cultured in sparse conditions, fibrin sprouts and scratch wound assays were fixed in methanol free 4 % formaldehyde (Thermo Fisher) and used in smFISH assays. Stellaris smFISH probes (Biosearch Technologies) targeting human *RAB13*, human *GAPDH* and zebrafish *RAB13* transcripts were purchased from Biosearch Technologies with Q570 and Q670 fluorophore modifications and used according to the manufacturer's manual.

Puro-PLA and immunofluorescence

Cell bodies of HUVECs cultured in Transwells were scraped and remaining protrusions were exposed to 3 µM Puromycin (Sigma) added to the lower chamber for 6 minutes. In translation inhibition

experiments, 40 µM Anisomycin (Sigma) was added to the lower Transwell chamber 30 min before cell body removal and 6 minutes after cell body removal together with 3 µM Puromycin. Subsequently, HUVEC protrusions grown in Transwell membranes were in fixed methanol free 4 % formaldehyde, removed from the Transwell inserts and used in immunofluorescence assays Puro-PLA experiments as described elsewhere (tom Dieck et al., 2015) using antibodies to detect RAB13 (Millipore) and Puromycin (Kerafast). Following the Puro-PLA protocol, Transwell membranes were incubated for 20 minutes with 1:40 Alexa Fluor 488 Phalloidin (Thermo Fisher) in PBS, washed in Duolink wash buffer B (Sigma) and mounted on microscope slides with Duolink *In Situ* Mounting Medium containing DAPI (Sigma).

For immunofluorescence, Transwell membranes were permeabilised in PBS (Sigma) containing 0.5% Triton-X100 (Sigma) and 4 % goat serum (Sigma) for 15 minutes, and blocked with 4 % goat serum in PBS at 4°C overnight. Next, membranes were incubated with 1:3500 Puromycin in blocking buffer at room temperature for 1 hour, washed in PBS and incubated with a goat anti-mouse AlexaFluor 568 antibody (Thermo Fisher) at room temperature for 1 hour. Membranes were incubated for 20 minutes with 1:40 Alexa Fluor 488 Phalloidin in PBS, washed in PBS and mounted on microscope slides with Vectashield antifade mounting medium containing DAPI (Vector Laboratories).

Plasmid construction

The 3' UTRs of human and zebrafish *RAB13* orthologues were amplified using sequence-specific primers Platinum Pfx DNA polymerase (Thermo Fisher) and cloned using a Zero Blunt PCR cloning kit (Thermo Fisher) following the manufacturer's manual. The 3' UTRs were sub-cloned into the BglII and SpeI sites in the pCR4-24XMS2SL-stable plasmid, a gift from Robert Singer (Addgene plasmid # 31865). In parallel, a multiple cloning site (MCS) was introduced using the same cloning sites.

For *in vitro* MS2 experiments, the human *HBB* gene was cloned into the NotI and BamHI sites in the pCR4-24XMS2SL-*RAB13* 3' UTR plasmid and the recombinant *HBB*-24XMS2SL-*RAB13* 3' UTR sequence was subcloned into the pcDNA3 mammalian expression vector (Thermo Fisher) using the NotI and XbaI sites. Deletion mutations of *RAB13* 3' UTR cloned Zero Blunt PCR were generated by PCR using Platinum Pfx DNA polymerase or using QuikChange II Site-Directed Mutagenesis kit (Agilent Technologies) following the manufacturer's instructions and introduced into the pcDNA3-*HBB*-24XMS2SL-MCS using NheI and XhoI sites.

In order to generate the zebrafish MS2 reporter construct, a Lyn-mCherry was inserted into pCR4-24XMS2SL-*rab13* 3' UTR using a EcorI site and the resulting Lyn-mCherry-24XMS2SL-*rab13* 3' UTR was amplified Platinum Pfx DNA polymerase and cloned into a pDONR221 P3-P2 using

Gateway Technology (Thermo Fisher) according to manufacturer's manual. The final Tol2-based construct was assembled into the pTol2Dest (Addgene plasmid # 73484) (Villefranc et al., 2007) using Gateway 3-fragment recombination with the following plasmids: pE(L1L4)Cerulean-H2B, pE(R4R3)basfli1ep and pE(L3L2) Lyn-mCherry-24XMS2SL-*rab13* 3' UTR.

To construct the Cerulean-H2B:bas*fli1ep:*MCP-GFPnls Tol2-based plasmid, MCP-GFPnls was amplified Platinum Pfx DNA polymerase from pMS2-GFP and cloned into a pDONR221 P3-P2. The final Tol2-based construct was assembled into the pTol2Dest using Gateway 3-fragment recombination with the following plasmids: pE(L1L4)Cerulean-H2B, pE(R4R3)basfli1ep and pE(L3L2) Lyn-mCherry-24XMS2SL-*rab13* 3' UTR.

Microscopy

Confocal time-lapse imaging of zebrafish was carried out as previously described (Costa et al., 2016). Images of cultured cells and Transwell membranes were acquired on an Olympus IX83 inverted microscope using Lumencor LED excitation, either a 40x/ 1.00 UplanApo or a 60x/ 1.42 PlanApo objective and a Sedat QUAD (DAPI/FITC/TRITC/Cy5) filter set (Chroma 89000). The images were collected using a R6 (Qimaging) CCD camera with a Z optical spacing of [0.2 – 0.3 μm]. Raw images were then deconvolved using the Huygens Pro software (SVI) and maximum intensity projections of these images were used for analysis.

Statistics

Statistical analysis of the data was carried out using GraphPad prism software, using parametric t-tests when the data were normally distributed or non-parametric Mann Whitney tests when the data did not pass normality tests.

REFERENCES

An, J.J., Gharami, K., Liao, G.Y., Woo, N.H., Lau, A.G., Vanevski, F., Torre, E.R., Jones, K.R., Feng, Y., Lu, B., *et al.* (2008). Distinct role of long 3' UTR BDNF mRNA in spine morphology and synaptic plasticity in hippocampal neurons. Cell *134*, 175-187.

Andreassi, C., Zimmermann, C., Mitter, R., Fusco, S., De Vita, S., Saiardi, A., and Riccio, A. (2010). An NGF-responsive element targets myo-inositol monophosphatase-1 mRNA to sympathetic neuron axons. Nat Neurosci *13*, 291-301.

Arima, S., Nishiyama, K., Ko, T., Arima, Y., Hakozaki, Y., Sugihara, K., Koseki, H., Uchijima, Y., Kurihara, Y., and Kurihara, H. (2011). Angiogenic morphogenesis driven by dynamic and heterogeneous collective endothelial cell movement. Development *138*, 4763-4776.

Aschrafi, A., Natera-Naranjo, O., Gioio, A.E., and Kaplan, B.B. (2010). Regulation of axonal trafficking of cytochrome c oxidase IV mRNA. Mol Cell Neurosci *43*, 422-430.

Bentley, K., Franco, C.A., Philippides, A., Blanco, R., Dierkes, M., Gebala, V., Stanchi, F., Jones, M., Aspalter, I.M., Cagna, G., *et al.* (2014). The role of differential VE-cadherin dynamics in cell rearrangement during angiogenesis. Nat Cell Biol *16*, 309-321.

Bertrand, E., Chartrand, P., Schaefer, M., Shenoy, S.M., Singer, R.H., and Long, R.M. (1998). Localization of ASH1 mRNA particles in living yeast. Mol Cell *2*, 437-445.

Bhuin, T., and Roy, J.K. (2014). Rab proteins: the key regulators of intracellular vesicle transport. Exp Cell Res *328*, 1-19.

Boyden, S. (1962). The chemotactic effect of mixtures of antibody and antigen on polymorphonuclear leucocytes. J Exp Med *115*, 453-466.

Brittis, P.A., Lu, Q., and Flanagan, J.G. (2002). Axonal protein synthesis provides a mechanism for localized regulation at an intermediate target. Cell *110*, 223-235.

Buxbaum, A.R., Haimovich, G., and Singer, R.H. (2015). In the right place at the right time: visualizing and understanding mRNA localization. Nat Rev Mol Cell Biol *16*, 95-109.

Campbell, P.D., Chao, J.A., Singer, R.H., and Marlow, F.L. (2015). Dynamic visualization of transcription and RNA subcellular localization in zebrafish. Development *142*, 1368-1374.

Chin, A., and Lecuyer, E. (2017). RNA localization: Making its way to the center stage. Biochim Biophys Acta *1861*, 2956-2970.

Costa, G., Harrington, K.I., Lovegrove, H.E., Page, D.J., Chakravartula, S., Bentley, K., and Herbert, S.P. (2016). Asymmetric division coordinates collective cell migration in angiogenesis. Nat Cell Biol *18*, 1292-1301.

Fusco, D., Accornero, N., Lavoie, B., Shenoy, S.M., Blanchard, J.M., Singer, R.H., and Bertrand, E. (2003). Single mRNA molecules demonstrate probabilistic movement in living mammalian cells. Curr Biol *13*, 161-167.

Gerhardt, H., Golding, M., Fruttiger, M., Ruhrberg, C., Lundkvist, A., Abramsson, A., Jeltsch, M., Mitchell, C., Alitalo, K., Shima, D., *et al.* (2003). VEGF guides angiogenic sprouting utilizing endothelial tip cell filopodia. J Cell Biol *161*, 1163-1177.

Harris, E.S., and Nelson, W.J. (2010). Adenomatous polyposis coli regulates endothelial cell migration independent of roles in beta-catenin signaling and cell-cell adhesion. Mol Biol Cell *21*, 2611-2623.

Herbert, S.P., and Stainier, D.Y. (2011). Molecular control of endothelial cell behaviour during blood vessel morphogenesis. Nat Rev Mol Cell Biol *12*, 551-564.

Hogan, B.M., and Schulte-Merker, S. (2017). How to Plumb a Pisces: Understanding Vascular Development and Disease Using Zebrafish Embryos. Dev Cell *42*, 567-583.

Ioannou, M.S., Bell, E.S., Girard, M., Chaineau, M., Hamlin, J.N., Daubaras, M., Monast, A., Park, M., Hodgson, L., and McPherson, P.S. (2015). DENND2B activates Rab13 at the leading edge of migrating cells and promotes metastatic behavior. J Cell Biol *208*, 629-648.

Isogai, S., Lawson, N.D., Torrealday, S., Horiguchi, M., and Weinstein, B.M. (2003). Angiogenic network formation in the developing vertebrate trunk. Development *130*, 5281-5290.

Jakobsen, K.R., Sorensen, E., Brondum, K.K., Daugaard, T.F., Thomsen, R., and Nielsen, A.L. (2013). Direct RNA sequencing mediated identification of mRNA localized in protrusions of human MDA-MB-231 metastatic breast cancer cells. J Mol Signal *8*, 9.

Jin, S.W., Beis, D., Mitchell, T., Chen, J.N., and Stainier, D.Y. (2005). Cellular and molecular analyses of vascular tube and lumen formation in zebrafish. Development *132*, 5199-5209.

Kislauskis, E.H., Zhu, X., and Singer, R.H. (1994). Sequences responsible for intracellular localization of beta-actin messenger RNA also affect cell phenotype. J Cell Biol *127*, 441-451.

Kislauskis, E.H., Zhu, X., and Singer, R.H. (1997). beta-Actin messenger RNA localization and protein synthesis augment cell motility. J Cell Biol *136*, 1263-1270.

Krause, M., and Gautreau, A. (2014). Steering cell migration: lamellipodium dynamics and the regulation of directional persistence. Nat Rev Mol Cell Biol *15*, 577-590.

Lee, I.Y., Kim, J., Ko, E.M., Jeoung, E.J., Kwon, Y.G., and Choe, J. (2002). Interleukin-4 inhibits the vascular endothelial growth factor- and basic fibroblast growth factor-induced angiogenesis in vitro. Mol Cells *14*, 115-121.

Liang, C.C., Park, A.Y., and Guan, J.L. (2007). In vitro scratch assay: a convenient and inexpensive method for analysis of cell migration in vitro. Nat Protoc *2*, 329-333.

Liao, G., Simone, B., and Liu, G. (2011). Mis-localization of Arp2 mRNA impairs persistence of directional cell migration. Exp Cell Res *317*, 812-822.

Mardakheh, F.K., Paul, A., Kumper, S., Sadok, A., Paterson, H., McCarthy, A., Yuan, Y., and Marshall, C.J. (2015). Global Analysis of mRNA, Translation, and Protein Localization: Local Translation Is a Key Regulator of Cell Protrusions. Dev Cell *35*, 344-357.

Marzesco, A.M., Dunia, I., Pandjaitan, R., Recouvreur, M., Dauzonne, D., Benedetti, E.L., Louvard, D., and Zahraoui, A. (2002). The small GTPase Rab13 regulates assembly of functional tight junctions in epithelial cells. Mol Biol Cell *13*, 1819-1831.

Mayor, R., and Etienne-Manneville, S. (2016). The front and rear of collective cell migration. Nat Rev Mol Cell Biol *17*, 97-109.

Mili, S., Moissoglu, K., and Macara, I.G. (2008). Genome-wide screen reveals APC-associated RNAs enriched in cell protrusions. Nature *453*, 115-119.

Miller, S., Yasuda, M., Coats, J.K., Jones, Y., Martone, M.E., and Mayford, M. (2002). Disruption of dendritic translation of CaMKIIalpha impairs stabilization of synaptic plasticity and memory consolidation. Neuron *36*, 507-519.

Moreno-Mateos, M.A., Vejnar, C.E., Beaudoin, J.D., Fernandez, J.P., Mis, E.K., Khokha, M.K., and Giraldez, A.J. (2015). CRISPRscan: designing highly efficient sgRNAs for CRISPR-Cas9 targeting in vivo. Nat Methods *12*, 982-988.

Nakatsu, M.N., and Hughes, C.C. (2008). An optimized three-dimensional in vitro model for the analysis of angiogenesis. Methods Enzymol *443*, 65-82.

Park, H.Y., Lim, H., Yoon, Y.J., Follenzi, A., Nwokafor, C., Lopez-Jones, M., Meng, X., and Singer, R.H. (2014). Visualization of dynamics of single endogenous mRNA labeled in live mouse. Science *343*, 422-424.

Park, H.Y., Trcek, T., Wells, A.L., Chao, J.A., and Singer, R.H. (2012). An unbiased analysis method to quantify mRNA localization reveals its correlation with cell motility. Cell Rep *1*, 179-184.

Pfeffer, S.R., Dirac-Svejstrup, A.B., and Soldati, T. (1995). Rab GDP dissociation inhibitor: putting rab GTPases in the right place. J Biol Chem *270*, 17057-17059.

Ruhrberg, C., Gerhardt, H., Golding, M., Watson, R., Ioannidou, S., Fujisawa, H., Betsholtz, C., and Shima, D.T. (2002). Spatially restricted patterning cues provided by heparin-binding VEGF-A control blood vessel branching morphogenesis. Genes Dev *16*, 2684-2698.

Sakane, A., Abdallah, A.A., Nakano, K., Honda, K., Ikeda, W., Nishikawa, Y., Matsumoto, M., Matsushita, N., Kitamura, T., and Sasaki, T. (2012). Rab13 small G protein and junctional Rab13-binding protein (JRAB) orchestrate actin cytoskeletal organization during epithelial junctional development. J Biol Chem *287*, 42455-42468.

Sakane, A., Alamir Mahmoud Abdallah, A., Nakano, K., Honda, K., Kitamura, T., Imoto, I., Matsushita, N., and Sasaki, T. (2013). Junctional Rab13-binding protein (JRAB) regulates cell spreading via filamins. Genes Cells *18*, 810-822.

Schedlich, L., Hill, M., and Lockett, T. (1997). Antisense inhibition of beta-actin mRNA localization and its effect on smooth muscle cell migration. Biol Cell *89*, 113-122.

Seabra, M.C., Mules, E.H., and Hume, A.N. (2002). Rab GTPases, intracellular traffic and disease. Trends Mol Med *8*, 23-30.

Shen, F., and Seabra, M.C. (1996). Mechanism of digeranylgeranylation of Rab proteins. Formation of a complex between monogeranylgeranyl-Rab and Rab escort protein. J Biol Chem *271*, 3692-3698.

Shestakova, E.A., Singer, R.H., and Condeelis, J. (2001). The physiological significance of beta -actin mRNA localization in determining cell polarity and directional motility. Proc Natl Acad Sci U S A *98*, 7045-7050.

Stuart, H.C., Jia, Z., Messenberg, A., Joshi, B., Underhill, T.M., Moukhles, H., and Nabi, I.R. (2008). Localized Rho GTPase activation regulates RNA dynamics and compartmentalization in tumor cell protrusions. J Biol Chem *283*, 34785-34795.

tom Dieck, S., Kochen, L., Hanus, C., Heumuller, M., Bartnik, I., Nassim-Assir, B., Merk, K., Mosler, T., Garg, S., Bunse, S., *et al.* (2015). Direct visualization of newly synthesized target proteins in situ. Nat Methods *12*, 411-414.

Villefranc, J.A., Amigo, J., and Lawson, N.D. (2007). Gateway compatible vectors for analysis of gene function in the zebrafish. Dev Dyn *236*, 3077-3087.

Wang, T., Hamilla, S., Cam, M., Aranda-Espinoza, H., and Mili, S. (2017). Extracellular matrix stiffness and cell contractility control RNA localization to promote cell migration. Nat Commun *8*, 896.

Wu, C., Agrawal, S., Vasanji, A., Drazba, J., Sarkaria, S., Xie, J., Welch, C.M., Liu, M., Anand-Apte, B., and Horowitz, A. (2011). Rab13-dependent trafficking of RhoA is required for directional migration and angiogenesis. J Biol Chem *286*, 23511-23520.

Wu, K.Y., Hengst, U., Cox, L.J., Macosko, E.Z., Jeromin, A., Urquhart, E.R., and Jaffrey, S.R. (2005). Local translation of RhoA regulates growth cone collapse. Nature *436*, 1020-1024.

Zahraoui, A., Joberty, G., Arpin, M., Fontaine, J.J., Hellio, R., Tavitian, A., and Louvard, D. (1994). A small rab GTPase is distributed in cytoplasmic vesicles in non polarized cells but colocalizes with the tight junction marker ZO-1 in polarized epithelial cells. J Cell Biol *124*, 101-115.

Zappulo, A., van den Bruck, D., Ciolli Mattioli, C., Franke, V., Imami, K., McShane, E., Moreno-Estelles, M., Calviello, L., Filipchyk, A., Peguero-Sanchez, E., *et al.* (2017). RNA localization is a key determinant of neurite-enriched proteome. Nat Commun *8*, 583.

FIGURE LEGENDS

Figure 1. *RAB13* mRNA is localised to protrusions in endothelial cells during migration.

(A) Scheme depicts the Transwell culture strategy. HUVECs cultured in the upper chamber extend protrusions through the Transwell membrane pores into the lower chamber containing VEGF-A.

(B) RNA-seq data are plotted in reads per kilobase of transcripts per million reads (RPKM) against fold change (FC) levels of protrusions over cell bodies; data are mean values represented in $\log_2$ (n=2 replicates).

(C) Bar graph representing qPCR analysis of mRNA enrichment in protrusions; data are mean±s.d. (n=3 replicates).

(D) smFISH detection of *RAB13* and *GAPDH* mRNA in an exemplar HUVEC; scale bar: 20 µm.

(E) Scatter plot shows the Polarisation Index of *GAPDH* and *RAB13* mRNA detected by smFISH in single HUVECs; lines are mean values (n=33 cells).

(F) smFISH analysis of *RAB13* and *GAPDH* mRNA distribution in an exemplar tip cell within a fibrin sprout; scale bar: 20 µm.

(G) Scatter plot represents the relative distance of *GAPDH* and *RAB13* mRNA centre of distribution to the nucleus in individual tip cells; lines are mean values (n=38 cells).

Figure 2. *RAB13* mRNA is translated in endothelial cell protrusions.

(A) Scheme depicts the strategy to label newly synthesised proteins in HUVEC protrusions formed in Tanswell cultures.

(B) Immunofluorescence detection of Puromycin incorporation into HUVEC protrusions present in the lower Transwell membrane side (representative of 3 replicates); scale bar: 10 µm.

(C) Puro-PLA analysis of newly synthesised RAB13 in HUVEC protrusions present in the lower Transwell membrane side (representative of 3 replicates); scale bar: 10 µm.

(D) Scatter plot shows the quantification of RAB13 Puro-PLA punctae number normalised to protrusion area; lines are mean values (n≥44 protrusions).

Figure 3. The 3' UTR of *rab13* localises transcripts to endothelial cell protrusions *in vivo*.

(A) bEnd.3 cells co-transfected with plasmids expressing Lyn-mCherry, MCP-GFPnls and 24xMS2-RAB13 3'UTR or 24xMS2- empty (representative of 21 cells); arrow: non-nuclear localisation of MCP-GFPnls; scale bars: 20 µm.

(B) Bar graph represents the percentage of bEND.3 cells with MCP-GFP localised to protrusions when co-transfected with deletion versions of *RAB13* 3'UTR tagged with 24x MS2 hairpins; data are mean±s.d. (n≥30 cells).

(C) smFISH analysis of representative Wt and Δ190 (Del) RAB13 3'UTR HUVECs; scale bar: 20 µm.

(D) Scatter plot shows the Polarisation Index of *GAPDH* and *RAB13* mRNA detected by smFISH in Wt and Del RAB13 3'UTR HUVECs; lines are mean values (n=10 cells); n.s. – non-significant.

(E) Representative time-lapse confocal micrographs of an ISV sprouting cell in a *Tg(fli1ep:MCP-GFPnls*) 28 hpf zebrafish embryo (time point 0 min); embryo injected at one cell stage with with *rab13* 3'UTR tagged with Lyn-mCherry and 24x MS2 hairpins; arrows: non-nuclear localisation of MCP-GFPnls; scale bars: 20 µm.

Figure 4. *RAB13* mRNA localisation regulates protrusion formation in angiogenesis *in-vivo*.

(A) smFISH analysis of representative cultured cells derived from wild type (+/+) and homozygous (-/-) *rab13* 3' UTR-deleted embryos; arrows: *rab13* mRNA; scale bar: 10 µm.

(B) Scatter plot shows the Polarisation Index of *rab13* mRNA detected by smFISH in individual *rab13* 3' UTR-deleted zebrafish cells; lines are mean values (n≥33 cells each genotype).

(C) Time-lapse confocal micrographs of representative *rab13* 3' UTR-deleted +/+ and -/- embryos starting at 25 hpf (time point 0 h); arrows: extra branches emerging from the main ISVs; DLAV– dorsal longitudinal anastomotic vessel, HM – horizontal myoseptum; scale bars: 50 µm.

(D) Schematic diagram representing the two most common types of extra branching observed in ISVs of zebrafish embryos.

(E) Bar graph shows the frequency of extra branching occurring at the horizontal myoseptum in *rab13* 3' UTR-deleted zebrafish embryos; data are mean±s.d. (n≥7 embryos each genotype).

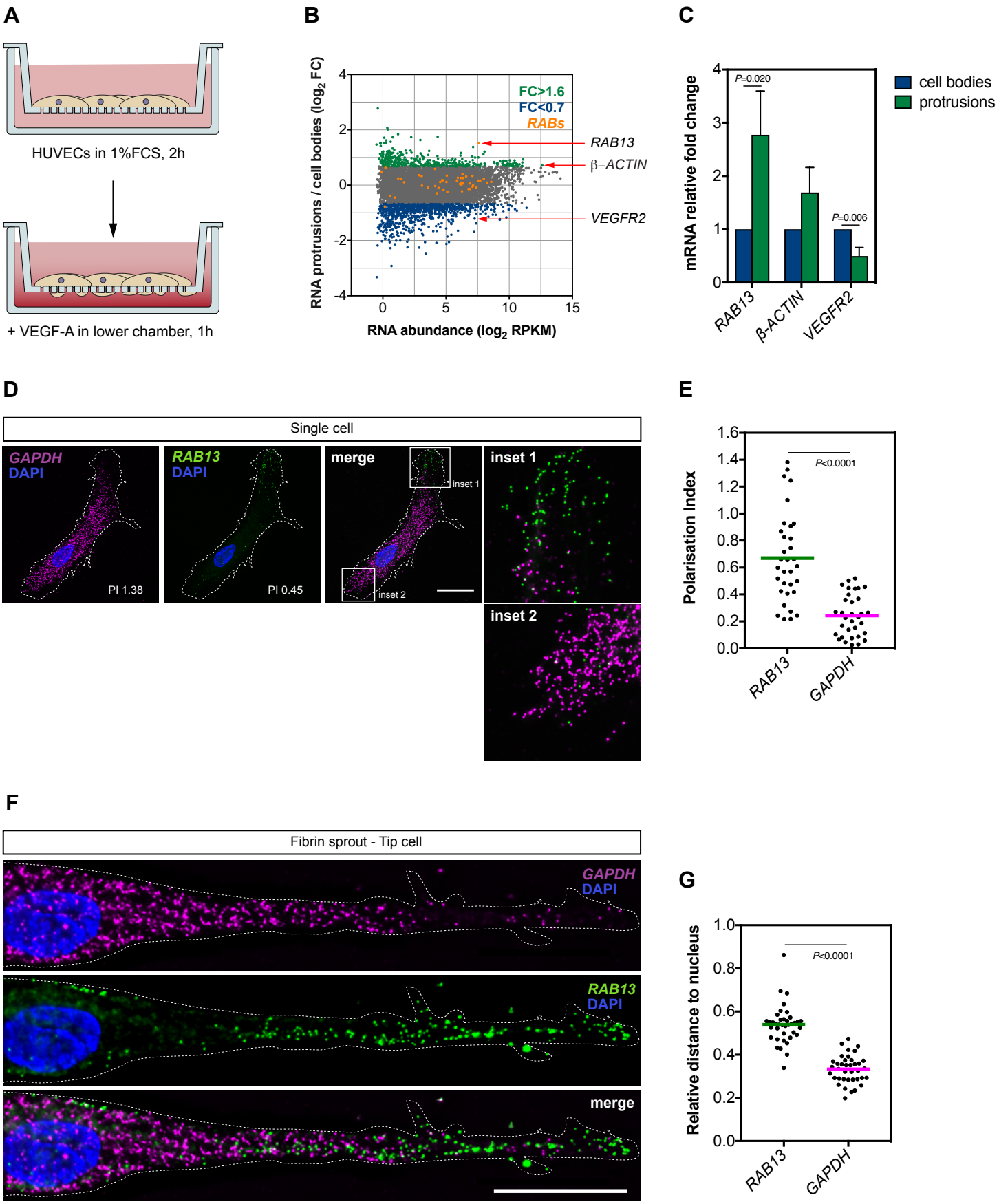
A
HUVECs in 1%FCS, 2h
+ VEGF-A in lower chamber, 1h
B
FC>1.6
FC<0.7
RABs
RAB13
β–ACTIN
VEGFR2
RNA protrusions / cell bodies (log2 FC)
RNA abundance (log2 RPKM)
C
P=0.020
P=0.006
cell bodies
protrusions
mRNA relative fold change
RAB13
β-ACTIN
VEGFR2
D
Single cell
GAPDH
DAPI
PI 1.38
RAB13
DAPI
PI 0.45
merge
inset 1
inset 2
E
P<0.0001
Polarisation Index
RAB13
GAPDH
F
Fibrin sprout - Tip cell
GAPDH
DAPI
RAB13
DAPI
merge
G
P<0.0001
Relative distance to nucleus
RAB13
GAPDH

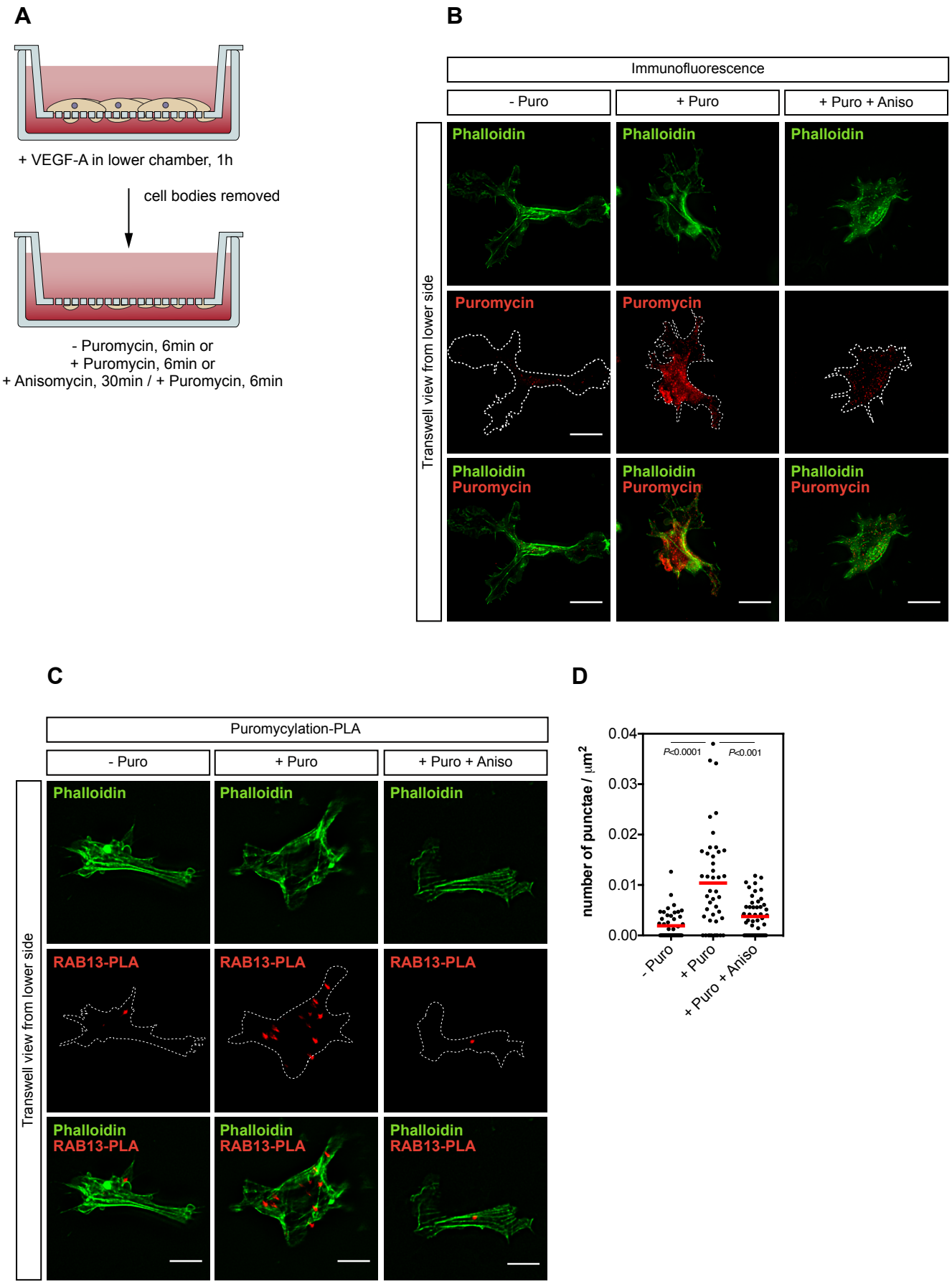
A
+ VEGF-A in lower chamber, 1h
cell bodies removed
- Puromycin, 6min or
+ Puromycin, 6min or
+ Anisomycin, 30min / + Puromycin, 6min
B
Immunofluorescence
- Puro
+ Puro
+ Puro + Aniso
Transwell view from lower side
Phalloidin
Puromycin
Phalloidin
Puromycin
C
Puromycylation-PLA
- Puro
+ Puro
+ Puro + Aniso
Transwell view from lower side
Phalloidin
RAB13-PLA
Phalloidin
RAB13-PLA
D
number of punctae / µm²
0.04
0.03
0.02
0.01
0.00
P<0.0001
P<0.001
- Puro
+ Puro
+ Puro + Aniso

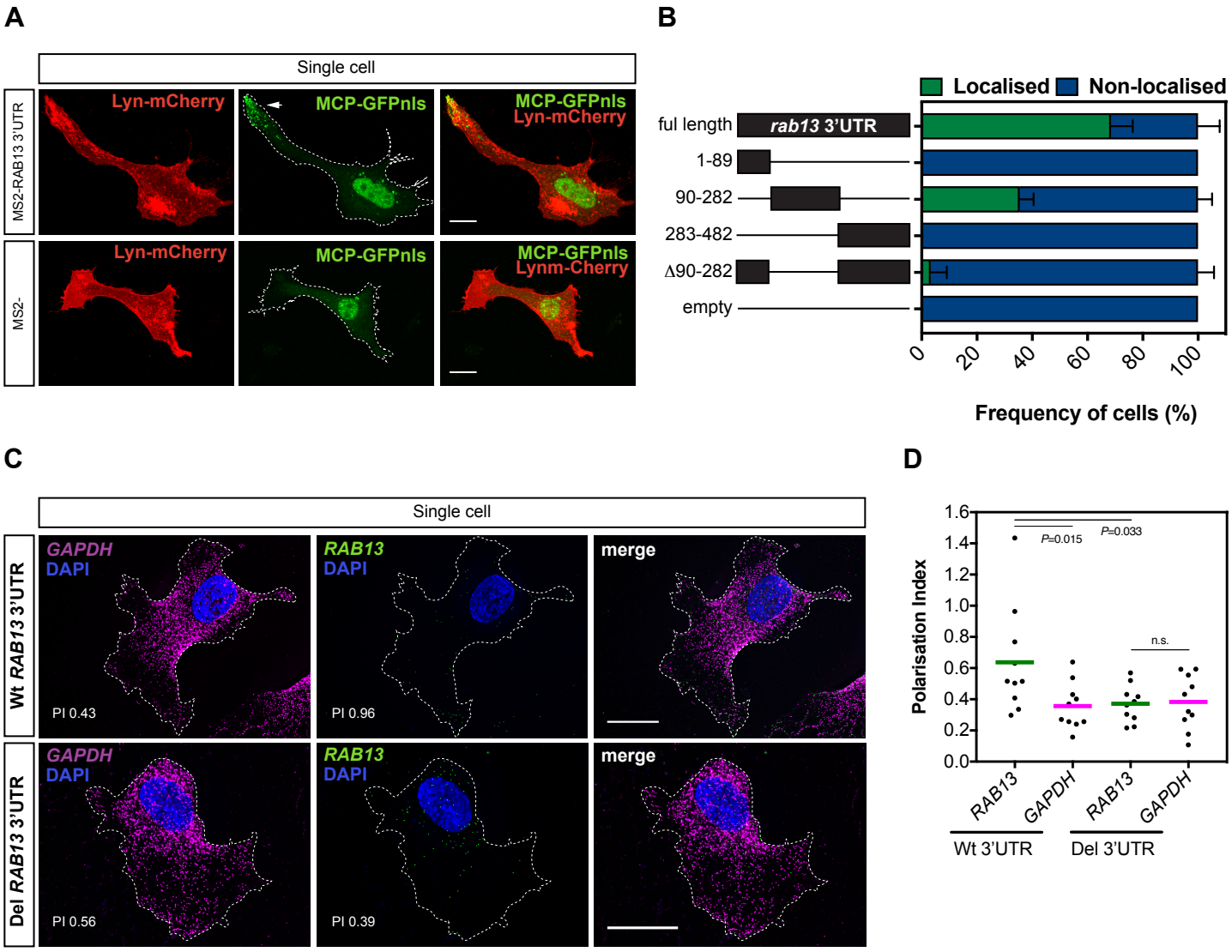
A
Single cell
MS2-RAB13 3'UTR
MS2-
Lyn-mCherry
MCP-GFPnls
MCP-GFPnls
Lyn-mCherry
Lyn-mCherry
MCP-GFPnls
MCP-GFPnls
Lynm-Cherry
B
Localised
Non-localised
ful length
rab13 3'UTR
1-89
90-282
283-482
Δ90-282
empty
0
20
40
60
80
100
Frequency of cells (%)
C
Single cell
Wt RAB13 3'UTR
Del RAB13 3'UTR
GAPDH
DAPI
RAB13
DAPI
merge
PI 0.43
PI 0.96
PI 0.56
PI 0.39
D
Polarisation Index
1.6
1.4
1.2
1.0
0.8
0.6
0.4
0.2
0.0
P=0.015
P=0.033
n.s.
RAB13
GAPDH
RAB13
GAPDH
Wt 3'UTR
Del 3'UTR

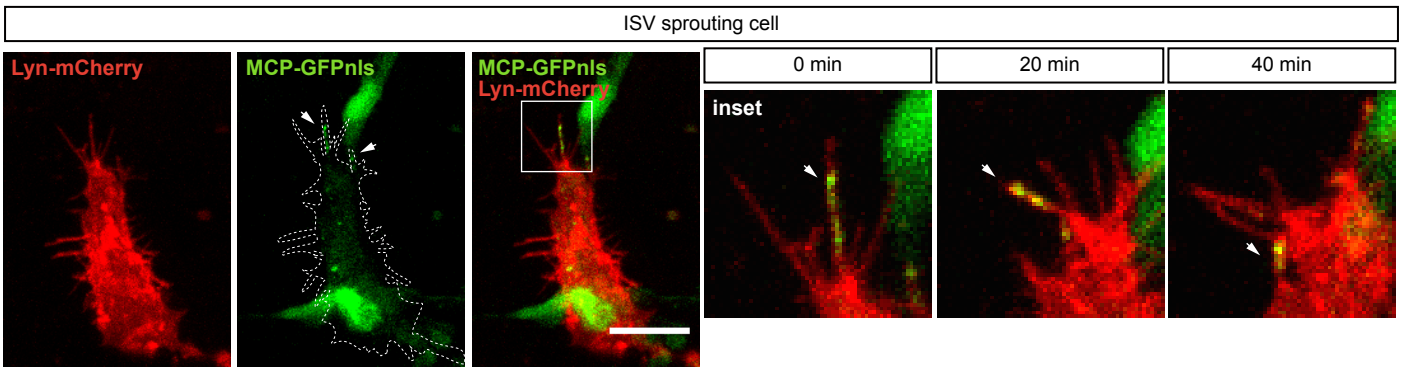
E
ISV sprouting cell
Lyn-mCherry
MCP-GFPnls
MCP-GFPnls
Lyn-mCherry
0 min
20 min
40 min
inset

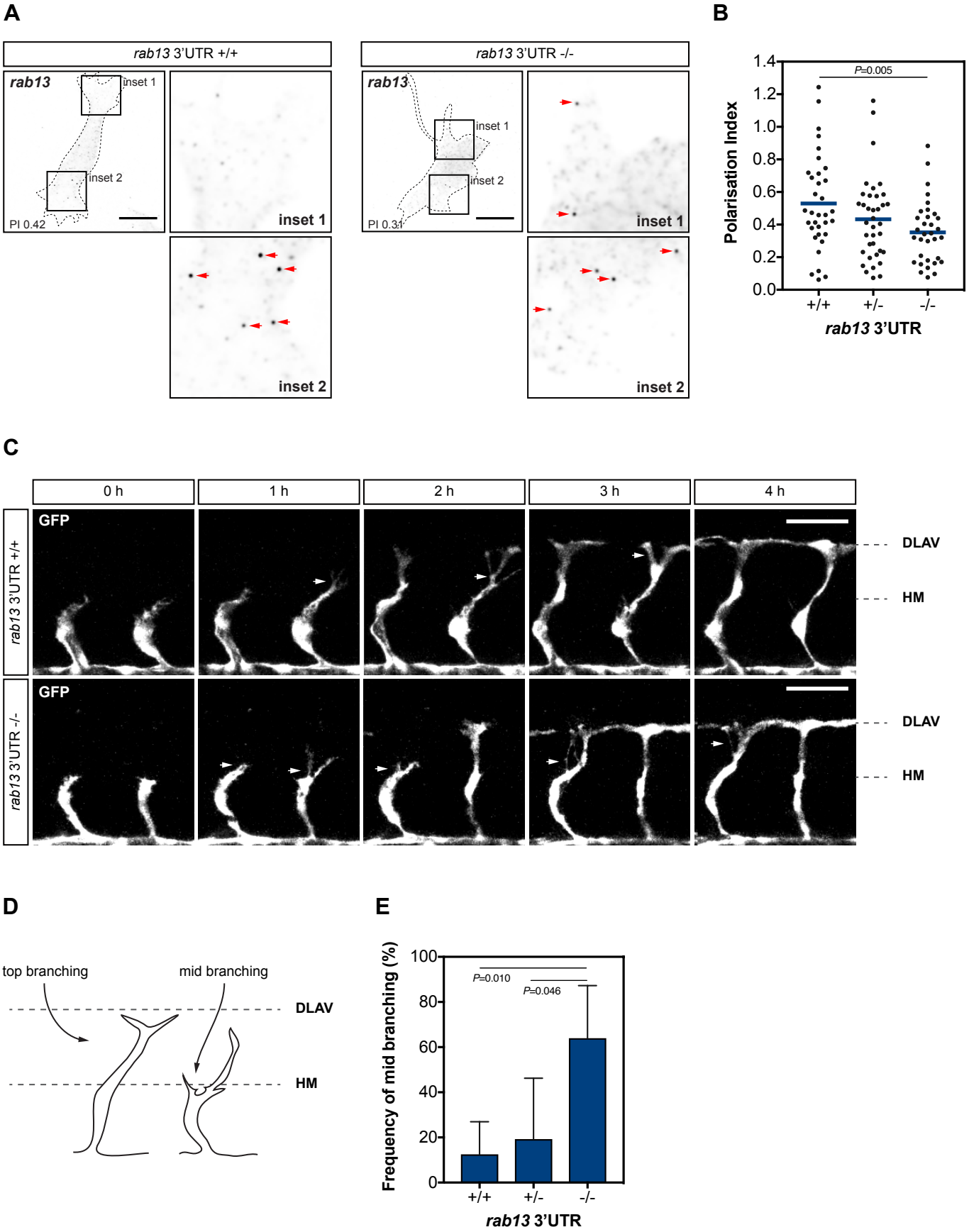
A
rab13 3'UTR +/+
rab13
inset 1
inset 2
PI 0.42
inset 1
inset 2
rab13 3'UTR -/-
rab13
inset 1
inset 2
PI 0.31
inset 1
inset 2
B
P=0.005
Polarisation Index
1.4
1.2
1.0
0.8
0.6
0.4
0.2
0.0
+/+
+/-
-/-
rab13 3'UTR
C
0 h
1 h
2 h
3 h
4 h
rab13 3'UTR +/+
rab13 3'UTR -/-
GFP
DLAV
HM
D
top branching
mid branching
DLAV
HM
E
P=0.010
P=0.046
Frequency of mid branching (%)
100
80
60
40
20
0
+/+
+/-
-/-
rab13 3'UTR